Q. J. R. Meteorol. Soc. (2000), **126**, pp. 2125–2142

Seasonal prediction of blocking frequency: Results from winter ensemble experiments

By V. PAVAN[1]*, S. TIBALDI[1] and Č. BRANKOVIĆ[2]
[1]*University of Bologna, Italy*
[2]*European Centre for Medium-Range Weather Forecasts, UK*

(Received 14 January 1999; revised 15 November 1999)

SUMMARY

The patterns which explain the largest fraction of the large-scale variability over the Euro–Atlantic and the Pacific regions are described using the National Centers for Environmental Prediction analysis data. In the description, special attention is given to the relation between these patterns and local weather regimes. The dynamical characteristics of each regime are found to be dependent on its relation with the basic flow over the region of its location.

The ability of the European Centre for Medium-Range Weather Forecasts T63L31 model in predicting the evolution of these large-scale patterns and associated weather regimes during winter is quantitatively estimated. The skill of the model prediction is shown to depend substantially on the pattern considered.

KEYWORDS: Blocking Ensemble simulations Seasonal predictability

1. INTRODUCTION

In recent years, much effort has been devoted to producing dependable seasonal forecasts. As far as extra-tropical regions are concerned, these efforts have been reasonably successful for North America. However, for Europe the level of success has been quite low; see, for example, Branković and Palmer (2000), Palmer and Anderson (1994), or Tracton *et al.* (1989). It has been argued that there might be two reasons for this outcome. On the one hand, the atmospheric flow over this region is characterized by low predictability due to its dynamical instability. On the other hand, its representation through the use of state-of-the-art general-circulation models (GCMs) is still affected by substantial systematic errors which might influence the modelled large-scale interannual and intra-seasonal variability.

From the dynamical point of view, Europe is situated at the exit region of the Atlantic storm-track, and its weather and climate are strongly influenced by the interannual and intra-seasonal variability of both the intensity and the extension of the mid-latitude jet stream. Many authors have described the observed large-scale variability over this region using sophisticated diagnostic tools (e.g. Legras and Ghil 1985; Vautard 1990; Plaut and Vautard 1994; Michelangeli *et al.* 1995). In all these studies, it was recognized that the tropospheric flow over Europe is substantially affected by the occurrence of quasi-stationary, persistent features, called 'blocks', which are able to shift, weaken or even interrupt the jet stream. It has also been recognized that the limited success achieved in medium- to extended-range forecasts over Europe is due to the inadequacy of the model performance in the representation of blocking onset and maintenance (Tracton *et al.* 1989).

Blocking onset is a regime transition characterized by low predictability (Tracton *et al.* 1989; Palmer and Anderson 1994). This implies that the exact time at which a regime transition takes place is mostly unpredictable beyond a few days. Several authors have shown how this is linked to the fact that one process responsible for blocking onset and maintanance is the upscale cascade of energy from transient eddies to quasi-stationary anomalies (blocks themselves) (e.g. Green 1977; Shutts 1986; Michelangeli and Vautard 1998). On the other hand, several authors pointed out that the occurrence

* Corresponding author: c/o CINECA, Via Magnanelli 6/3, Casalecchio di Reno, 40033 Bologna, Italy.

of blocking over the Euro–Atlantic region is favoured by the presence of particular extra-tropical large-scale anomalies. For example, Nakamura *et al.* (1997) suggest that, while the interaction between quasi-stationary and transient features is essential to both onset and maintenance of blocking over the Pacific, over the Atlantic the planetary waves seem to play a central and more substantial role. These results are supported by Ferranti *et al.* (1994) who documented a correlation between anomalously high sea surface temperature (SST) in the west tropical Pacific and the occurrence of blocking in the Euro–Atlantic region. Finally, Hoskins and Sardeshmukh (1987) envisage that one important ingredient, for an adequate representation of blocking events over Europe, is the correct reproduction of the Rossby-wave source associated with large SST anomalies in the equatorial Atlantic. These findings open up the possibility of predicting, with some confidence, the frequency of blocking events on seasonal time-scales. Although these results might make the problem at hand more feasible, it is necessary to remember that strong nonlinear interactions between transients and quasi-stationary waves might come into play, making our problem more complex.

In this paper, after describing the dataset and the diagnostic tools employed in our analysis in section 2, in section 3 we identify the most relevant patterns of large-scale variability over the northern hemisphere and describe their relation with the occurrence of blocking. In section 4 we quantify the skill of the European Centre for Medium-Range Weather Forecasts (ECMWF) model in predicting the frequency of blocking events using ensemble seasonal simulations. A more detailed description of the model results is given in section 5, and all results are summarized in section 6.

2. Data and diagnostic tools

(*a*) *Datasets*

The results presented in this work are obtained by analysing both observational and model data. The observational data are taken from the National Centers for Environmental Prediction (NCEP) analysis, and from the ECMWF re-analysis (ERA).

The NCEP analysis provides daily data for the period from 1946 to 1994, and is defined on an octagonal regular grid with 1977 points covering the northern hemisphere from 20°N to the north pole. We extracted from this dataset monthly mean 500 mb geopotential height (Z500) interpolated onto a 2.5° × 2.5° regular grid. The main deficiencies of the NCEP dataset are its coarse spatial resolution and its inhomogeneity in time, since the model used to produce it has undergone several changes during the years. However, the dataset is the only one available to us spanning a sufficiently large number of years to give a satisfactory statistical significance to our results, especially in the case of the pattern associated with European blocking (D'Andrea *et al.* 1998) and it has been shown to be sufficiently dependable for weather regime studies by several authors.

The ERA data are available for the years from 1979 to 1994 (Gibson *et al.* 1997), and include several daily and monthly mean fields. We have used upper-air fields and sea-level pressure (SLP) on a 2.5° × 2.5° regular grid and surface monthly cumulated fields (surface heat fluxes, precipitation, etc.) on the original 1.125°×1.121° Gaussian grid.

The ECMWF model data are wintertime, 1979/80 to 1992/93, seasonal ensembles, part of the European Programme on Prediction of Climate Variations on Seasonal and Interannual Time-scales (PROVOST). Each ensemble is composed of nine integrations made using cycle 13r4 of the ECMWF model, at T63 resolution with 31 model levels (Branković and Palmer 2000). The SSTs used to force the model were updated daily and

were obtained through interpolation from monthly ERA SSTs. The integrations were initialized using re-analysis data for nine subsequent days starting from 20 November each year and were extended to the last day of March of the following year. In order to avoid dependence on initial conditions, verification of model results is done only for the months of January, February and March (JFM).

(*b*) *Diagnostics*

The work starts with a standard empirical orthogonal function (EOF) analysis on the NCEP Z500 monthly anomalies for the months December–March (DJFM). The EOF analysis was performed separately in two different areas: the Euro–Atlantic sector (from 90°W to 60°E and from 20°N to the north pole) and the Pacific sector including North America (from 110°E to 70°W and from 20°N to the north pole).

The blocking and storm frequencies for each month were computed from daily data from ERA. Following Tibaldi and Molteni (1990) and Corti *et al.* (1997), blocking frequency is defined as a function of longitude, as the proportion of days in which easterlies occur in a latitudinal band between 40°N and 60°N, while westerlies exceeding 5 m s^{-1} are present north of 60°N.

Intense-storms frequency is obtained by counting the number of minima of high-pass filtered SLP, passing a given longitude between 20°N and 90°N, each month. Filtering is obtained by removing the three-day running mean, and only minima with intensities greater than 10 mb are retained, in order to identify clearly the storm tracks.

3. Analysis of observational data

(*a*) *Patterns of low-frequency variability*

The first four Euro–Atlantic EOFs (ATL-EOF1, ATL-EOF2, ATL-EOF3, and ATL-EOF4) of the DJFM Z500 monthly anomaly covariance matrix explain about 70% of variance. In Fig. 1, we show covariances between the four associated principal components (PCs) and the Z500 anomalies from ERA. This allows us to identify the main characteristics of these patterns during the years covered by the seasonal forecasts presented here. The patterns have been thoroughly described in Pavan *et al.* (2000), hereafter referred to as PMB, and here, for brevity, we limit our discussion to the main results presented there.

ATL-EOF1 (31% of the variance) is representative of the North Atlantic Oscillation pattern (NAO; see Barnston and Livezey (1987) for a definition based on mid-tropospheric height).

ATL-EOF2 (17% of the variance) is similar to the 500 mb height eastern Atlantic pattern described by Wallace and Gutzler (1981).

ATL-EOF3 (12% of the variance) is the most spatially confined of the four patterns. In its negative phase, it bears a strong resemblance to the composite maps of Euro–Atlantic blocking shown by Tibaldi and Molteni (1990) and Tibaldi *et al.* (1994). The intra-seasonal variability of this pattern is larger than its interannual variability: the ratio between the two is equal to 2.5 (substantially larger than the corresponding ratio for EOF1, which is equal to 1.7). This suggests that the value of the third PC (ATL-PC3) can vary substantially from one month to the next within the same winter, so that the occurrence of European blocking is either preceded or followed by months in which the Atlantic jet is particularly intense and extended eastward, in accordance with the results presented by Vautard (1990). It is also possible to define an index of extreme events over the north-eastern Atlantic sector, defined as the seasonal average of the absolute values of PC3. This index presents a secular trend similar to that observed in the NAO (Hurrel

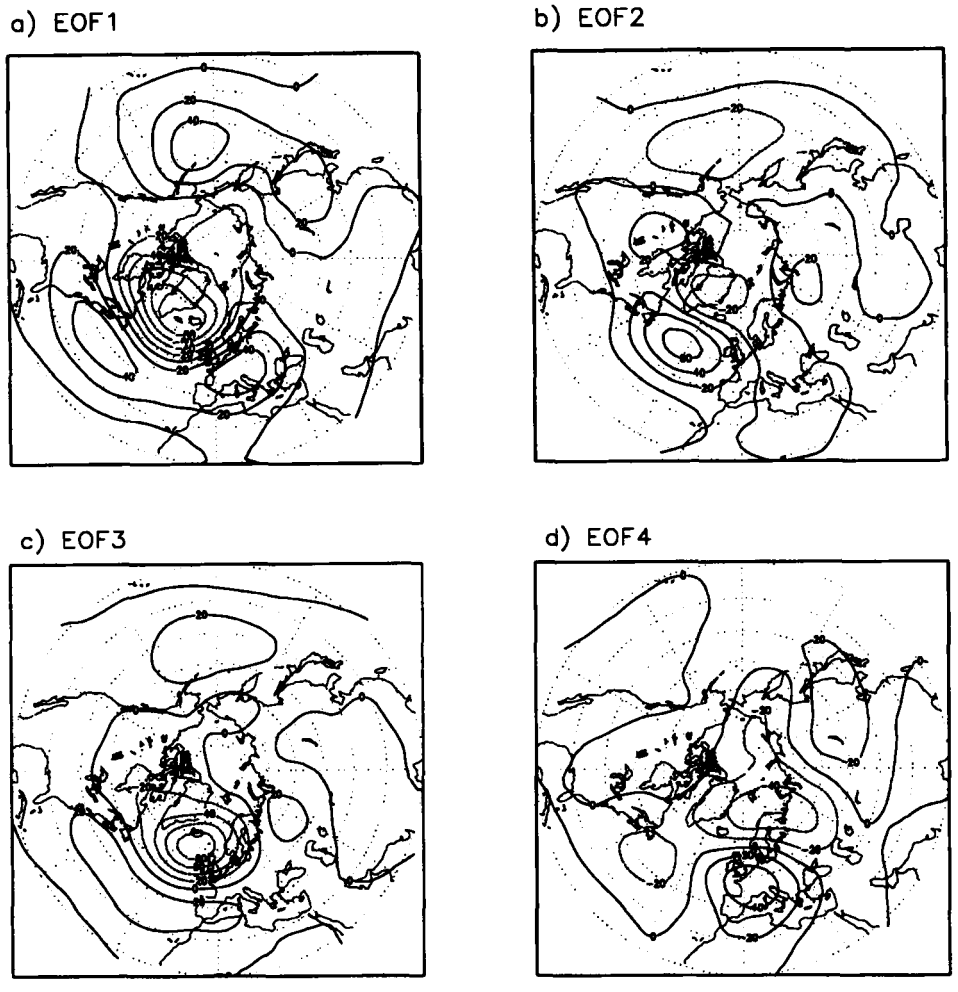

Figure 1. Covariances between (a) ATL-EOF1, (b) ATL-EOF2, (c) ATL-EOF3, and (d) ATL-EOF4 and 500 mb geopotential-height anomalies from ECMWF re-analyses. Contour intervals are every 20 m. Negative contours are dashed. (See text for further explanation.)

1996; Hurrel and van Loon 1997), but the correlation between the two is only 0.29, suggesting that although the two indices show a similar secularity, their interannual variabilities are not too closely correlated. It is interesting to notice that the value of this correlation for the 14 years of the winter ensemble (WE), is equal to 0.85. This confusing result might be related to the strong decadal variability of the two indices, and to the concurrence of large trends during the last 20 years, widely documented in the literature.

Finally, ATL-EOF4 (10% of the variance, Fig. 1(d)) is similar to the Eurasian type-1 pattern of Barnston and Livezey (1987), and also shares some features with either the SENA (Southern Europe–North Atlantic) or the SCAN (Scandinavian) patterns defined by Rogers (1990). Both ATL-EOF2 and ATL-EOF4 are strongly correlated with 'El-Niño' SST anomalies (see PMB).

The first four Pacific EOFs (PAC-EOF1 to 4) together explain more than 60% of the total wintertime 500 mb geopotential-height large-scale variance over this region.

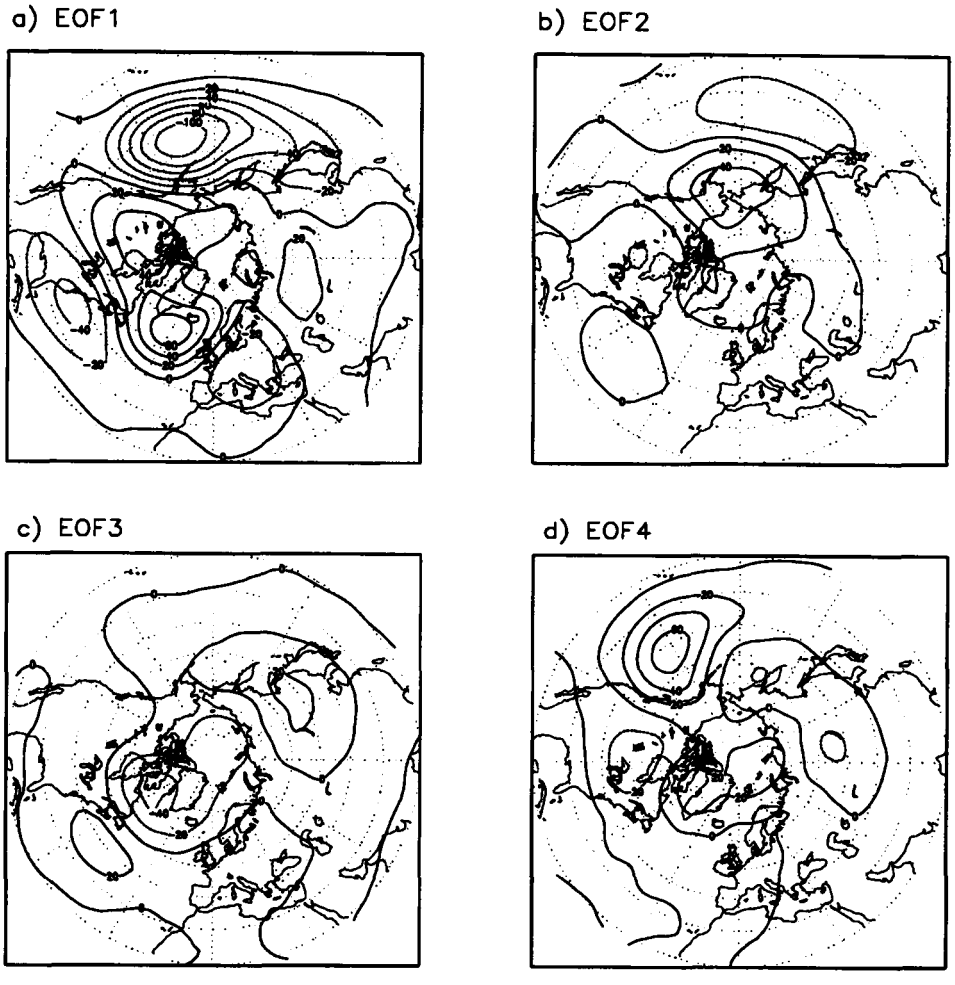

Figure 2. Covariances between (a) PAC-EOF1, (b) PAC-EOF2, (c) PAC-EOF3, and (d) PAC-EOF4 and 500 mb geopotential-height anomalies from ECMWF re-analyses. Contour intervals are every 20 m. Negative contours are dashed. (See text for further explanation.)

In Fig. 2, we show the covariances between these patterns and the northern hemisphere Z500 monthly anomalies from ERA.

PAC-EOF1, which explains 27% of the total variance, resembles closely the Pacific/North American pattern (PNA; e.g. Wallace and Gutzler 1981; Dole 1986; Barnston and Livezey 1987; Kimoto and Ghill 1993).

The positive phase of PAC-EOF2, which explains 16% of the total variance, strongly resembles the pattern of Pacific Ω-shaped blocks centred over the Aleutians described in Kimoto and Ghill (1993). Its negative phase produces a northward shift of the mid-latitude Pacific jet, and it resembles a northward-shifted PNA pattern. This pattern is also similar to the West Pacific pattern of Wallace and Gutzler (1981) and the West Pacific Oscillation of Barnston and Livezey (1987), and, together with the PNA pattern, has also been reproduced in some idealized studies, such as using a simple quasi-geostrophic model (e.g. Molteni and Corti 1998).

PAC-EOF3, which explains 12% of the total variance, has a pattern very similar to the NAO, reaching its maximum amplitude over Greenland. The similarity between

the PAC-EOF3 and the ATL-EOF1 patterns is confirmed by the high correlation, 0.69, between the corresponding Pacific and Atlantic PCs, describing their time evolution. This result is interesting for many reasons. First, the rank of this mode of variability over the Atlantic region suggests that the constraint of mathematical orthogonality does not interfere with the identification of this pattern in the Pacific region. Therefore, in our analysis the pattern emerges as an independent mode of variability, both dynamically and spatially distinguished from other local modes like, for example, the PNA pattern. This suggests the substantial independence of the NAO from an oscillation based on equatorial Pacific forcing which, as mentioned above, has high a correlation with the PNA tropospheric anomaly pattern. Second, the identification of the NAO as a mode of oscillation, not only of the Atlantic region but also of the Pacific region, highlights its planetary character, in agreement with Wallace and Gutzler (1981) who found that the NAO can be considered as an oscillation in the intensity of the northern-hemisphere zonal-mean flow, which amplifies and shifts the eddy part of the large-scale flow over the North Atlantic region. This interpretation is supported by a strong similarity between the Z500 anomaly pattern and the tropospheric response to mid-latitude thermal and/or orographic forcing shown by Hoskins and Karoly (1981). Also, recently Thompson and Wallace (1998) identified the existence of a hemispheric mode of oscillation of the zonal index, which they called the Arctic Oscillation (AO). The AO is recovered by them as the first mode of variability in SLP and of 100 mb geopotential height.

Finally, PAC-EOF4, which explains 9% of the total variance, is quite localized and represents an intensification (or a weakening) of the stationary eddy component of the north Pacific large-scale flow climatology. The positive phase of this pattern suggests an intensification of the Pacific jet off the east coast of Asia, associated with an increase in the same quantity just upstream of the Rocky Mountains. The negative phase of this pattern produces an intensification of blocking frequency at the exit region of the Pacific jet, and strongly resembles the North Pacific anomaly described by Dole (1983).

(*b*) *Correlation between EOFs and local weather regimes*

In this subsection, we discuss the correlation between the regional EOF patterns just describd and local weather regimes. We limit our discussion to ATL-EOF1, ATL-EOF3, ATL-EOF4, PAC-EOF2 and PAC-EOF4 which are the most highly correlated with the occurrence of blocking. In Fig. 3 the composites of the monthly blocking frequencies, computed using daily Z500 ERA for those months in which each of the considered PCs is larger than 0.67 or smaller than −0.67, are shown. For comparison, we show also the climatology as a solid line. The threshold value of 0.67 was chosen because the integral of the normal gaussian distribution over the interval going from −0.67 to 0.67 is equal to 0.5.

Each of the EOFs is associated with changes in blocking frequency localized over its sector of definition, confirming the results anticipated by looking at the Z500 covariance patterns. In some cases (ATL-EOF3, ATL-EOF4 and PAC-EOF4) a change in frequency is also observed over the remaining part of the hemisphere. While the correlations over the sector of definition of each EOF are robust and their values remain unaltered when considering longer time series of blocking frequencies, such as those obtainable using NCEP analysis, the same does not hold for the correlations over the remaining part of the globe. This reveals that the occurrence of blocking events over both ocean basins at the same time may have a weak significance or may be related to the strong decadal variability of large-scale anomalies. In the case of PAC-EOF4 the signal is distinctly nonlinear, with a substantial intensification with respect to climatology in the number of blocks occurring over the Pacific in one phase, but a negligible decrease in blocking

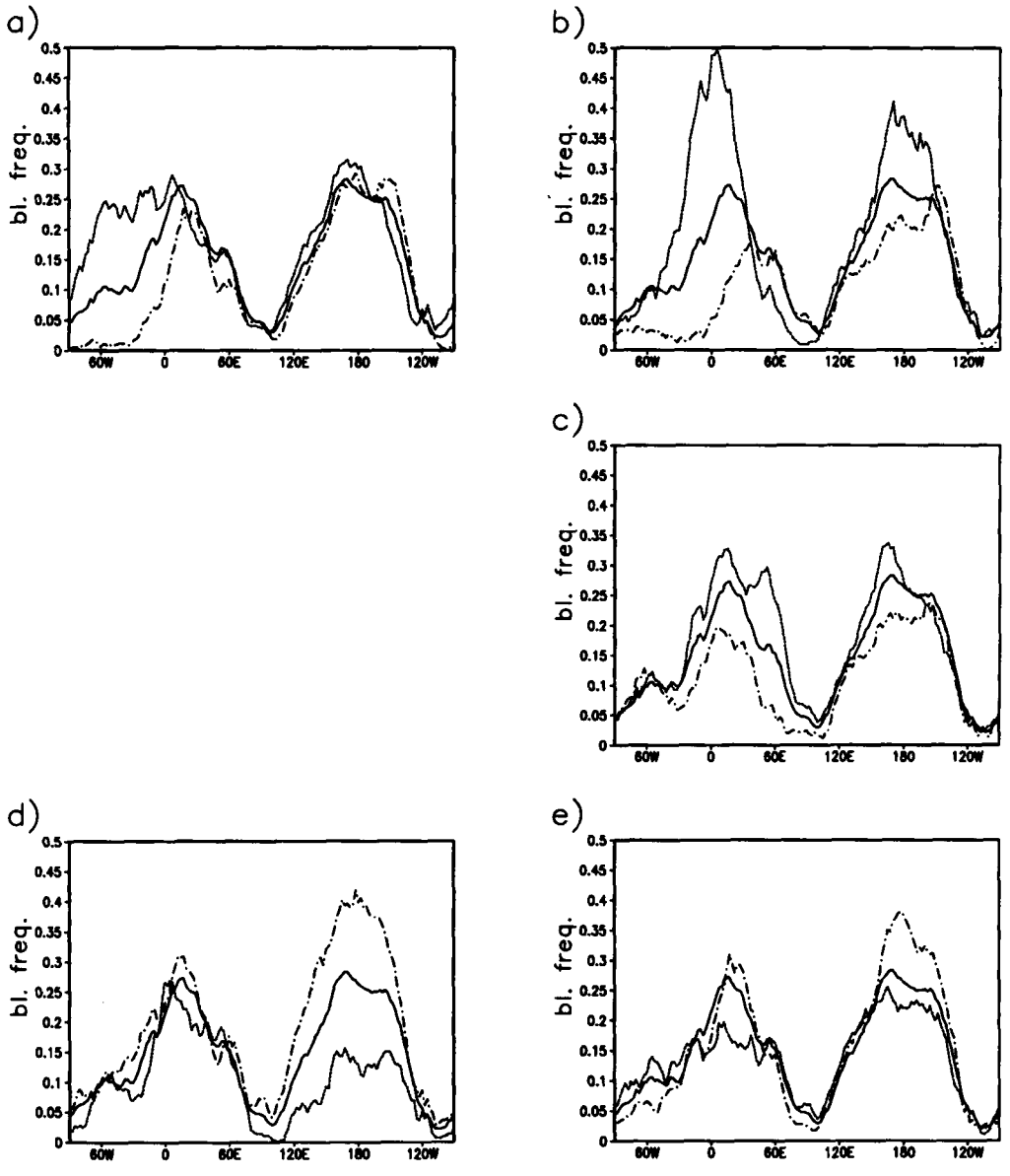

Figure 3. Climatology (solid line) and composites of ECMWF re-analyses blocking frequency for months in which one principal component is larger than 0.67 (dashed-dotted line) or smaller than −0.67 (dotted line), for (a) ATL-EOF1, (b) ATL-EOF3, (c) ATL-EOF4, (d) PAC-EOF2 and (e) PAC-EOF4. (See text for further explanation.)

frequency when the opposite phase of the same patterns occurs. In all other cases we notice a linear behaviour.

In Fig. 4, we show the composites of cyclone frequencies for the same patterns, computed using the same criteria as for blocking frequency. All composites present quite noisy anomalies of cyclone frequency in association with the occurrence of each large-scale pattern, but the features we are going to identify are robust and independent both in the frequency of the data used to compute the frequencies (results were obtained both for once- and for twice-daily data) and in the extension of the dataset (similar results

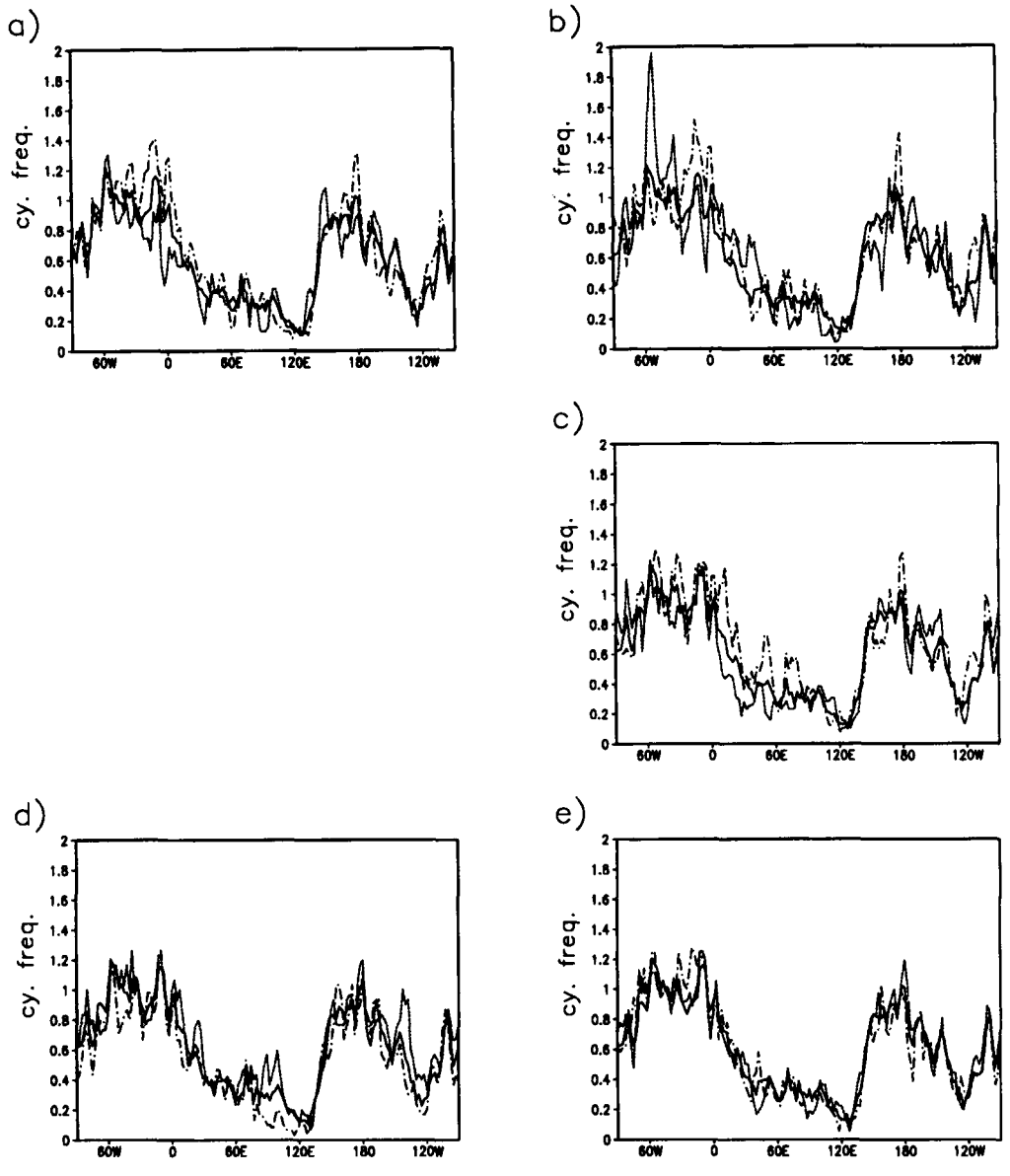

Figure 4. Same as Fig. 3 but for composites of ECMWF re-analysis cyclone frequency.

were obtained using the NMC analysis data). In most cases greater (smaller) values of blocking frequency are associated with smaller (greater) values of cyclone frequencies over the same region. In the case of European blocking (ATL-EOF3) we notice a substantal increase in the frequency of storms just upstream of the blocking region. This result confirms the relevance of the eddy transport of low potential vorticity (PV) in the maintenance of blockings located at the end of the Atlantic storm-track in agreement with the theory of Shutts (1986), Green (1977) and with the work by Michelangeli and Vautard (1998). This result does not hold for the blocking associated with the ATL-EOF1 pattern, which is maintained through a different dynamical mechanism.

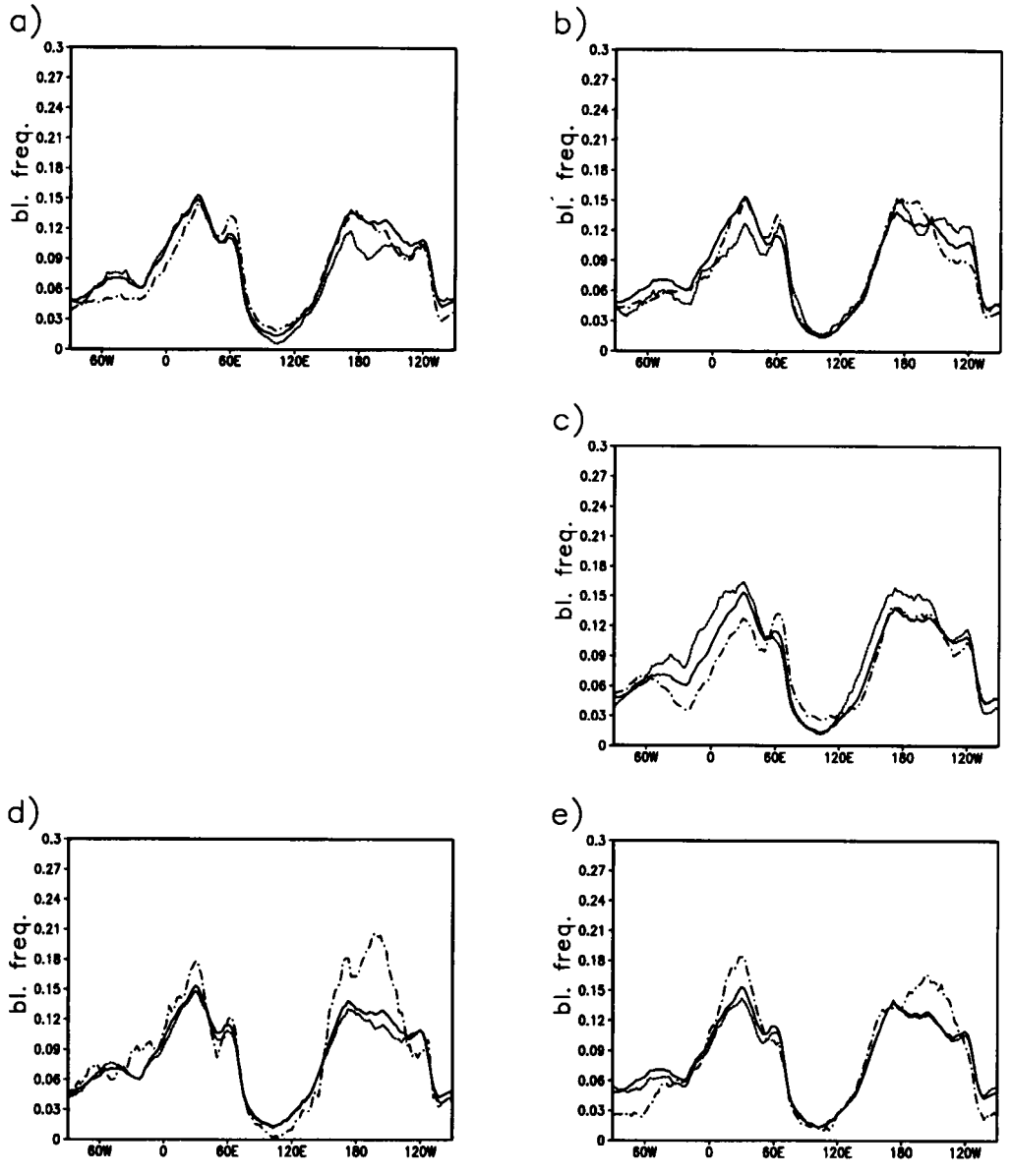

Figure 5. Climatology (solid line) and composites of model blocking frequency for months in which one principal component is larger than 0.67 (dashed-dotted line) or smaller than −0.67 (dotted line) for (a) ATL-EOF1, (b) ATL-EOF3, (c) ATL-EOF4, (d) PAC-EOF2 and (e) PAC-EOF4. (See text for further explanation.)

4. Analysis of Model Simulations

In order to evaluate the ability of the model to adequately forecast blocking frequency variability we show in Fig. 5 the composites of blocking frequency obtained including all the ensemble member results for those months in which the observed projection over one chosen EOF is larger than 0.67 or smaller than -0.67. The graph convention is the same as in Fig. 3, in order to make the comparison easier. We notice that the model is biased towards low values of blocking frequencies. This zonal bias has

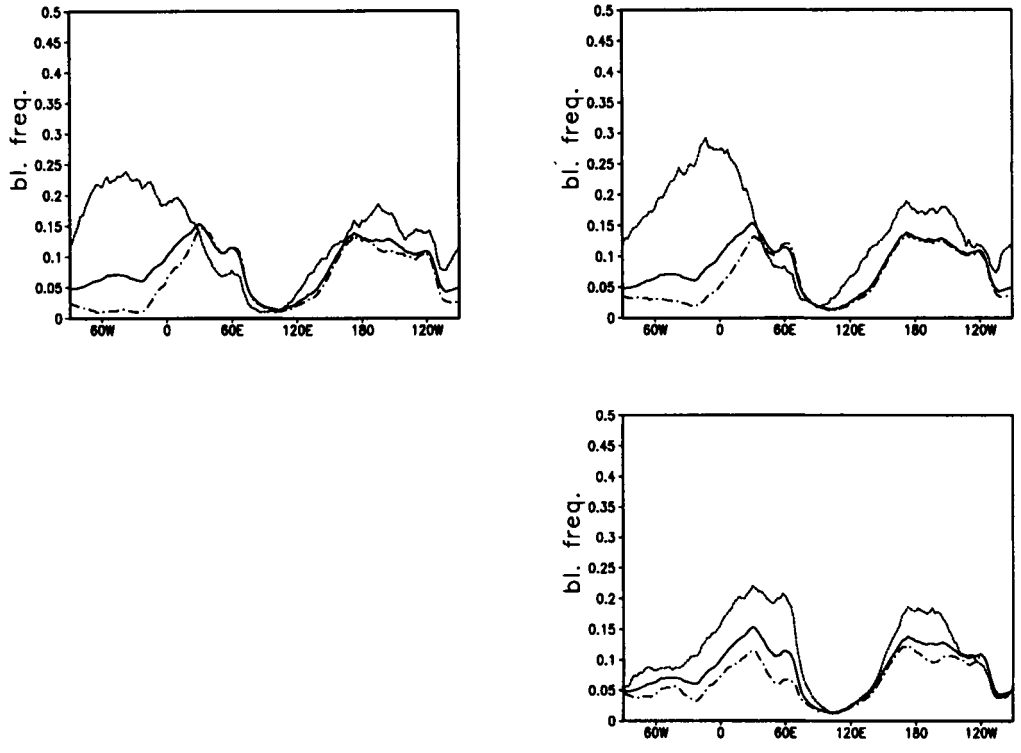

Figure 6. Climatology (solid line) and composites of model blocking frequency for those months in which each winter ensemble member has a projection on the empirical orthogonal function larger than 0.67 (dashed-dotted line) or smaller than −0.67 (dotted line), for (a) ATL-EOF1, (b) ATL-EOF3 and (c) ATL-EOF4. (See text for further explanation).

TABLE 1. CORRELATION BETWEEN FORECASTED AND OBSERVED ABSOLUTE VALUES OF PROJECTIONS ON THE FOUR EURO–ATLANTIC EMPIRICAL ORTHOGONAL FUNCTIONS (EOF1–4).

	EOF1	EOF2	EOF3	EOF4
Correlation	0.83	0.29	0.58	0.21

been observed by many authors and is a common feature of several different models (Ferranti *et al.* 1994; Branković and Molteni 1997; Pavan and Doblas-Reyes 2000). The model is able to capture the sign, if not the amplitude, of the signal in the case of the Pacific patterns and it does so for ATL-EOF4. It has problems in reproducing the linear behaviour of the large-scale flow in the case of the two opposite phases of PAC-EOF2, and in general in reproducing the variabilities of both NAO and European blocking.

A relatively poor model performance over the Euro–Atlantic region may be associated with a complete inability of the model to reproduce these blocking patterns. To check this hypothesis we verified that, when the model produces a large-scale pattern similar to the one characterizing blocking over the Euro–Atlantic area, the amplitude of the model blocking frequency compares well with the composites shown in Fig. 3. We computed composites of the model blocking frequency for those months of each ensemble member whose projections onto a chosen pattern are larger than 0.67 or smaller

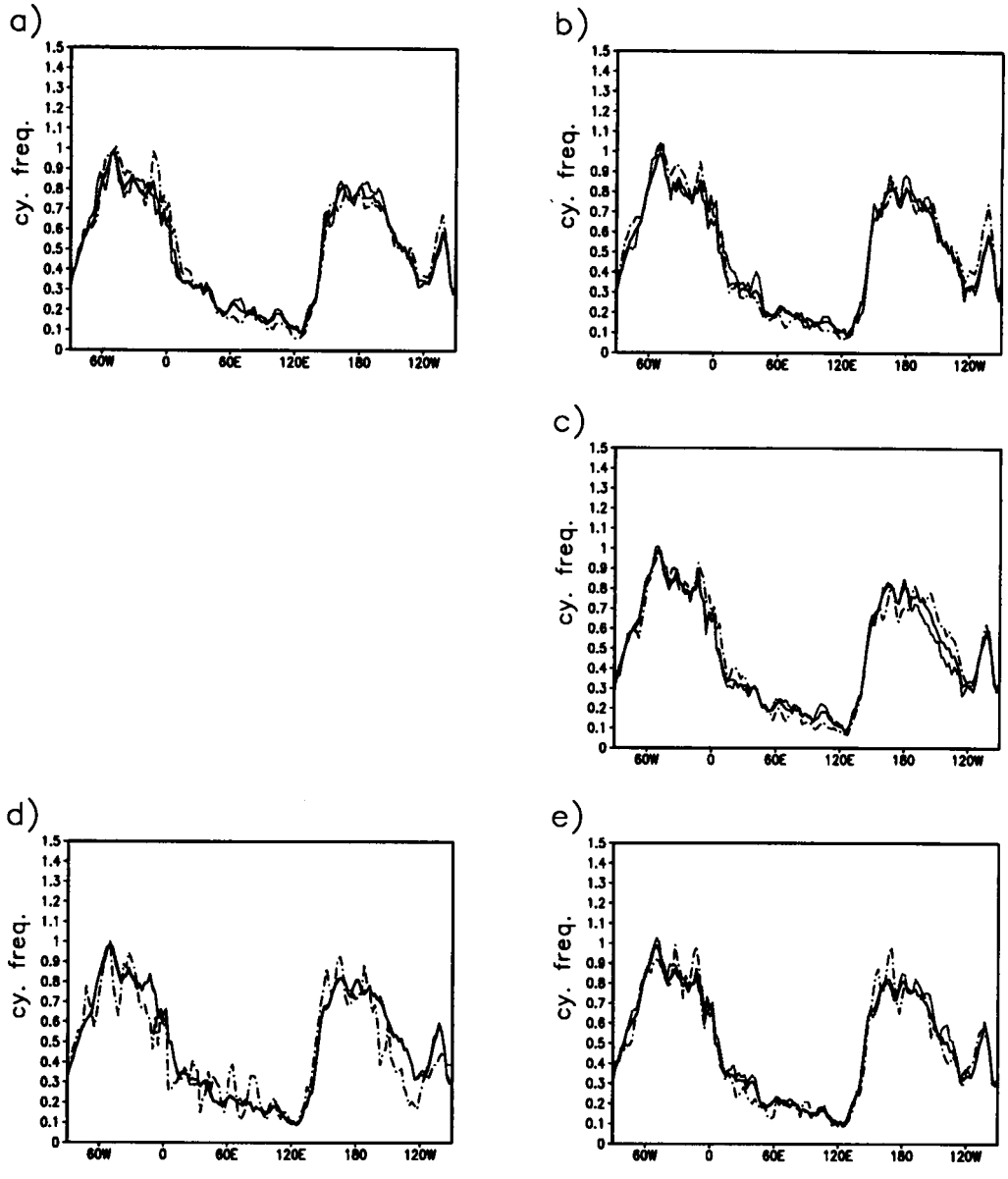

Figure 7. Same as Fig. 6 but for composites of model cyclone frequency.

than −0.67. These composites allow us to identify the value of model blocking frequency only when the model itself is able to reproduce large-scale anomalies similar or opposite to each of the EOFs. These composites for the Euro–Atlantic patterns (EOF1, EOF3 and EOF4) are shown in Fig. 6. A comparison between Fig. 6 and Fig. 3 shows good agreement between model and observations. However, the number of cases used to compute each of these blocking composites is small for the European blocking when compared with the other patterns, suggesting a deficiency in the statistical population from which this particular composite is computed.

We conclude that, although the distribution of the block forecast is strongly biased, the model is able to reproduce the main features of the observed flow in a very limited number of cases.

In section 3 we introduced the index of extreme events for ATL-EOF3 as the absolute value of the corresponding PC. We want to verify the model forecast for the JFM winter average of this index for all the PCs of the Euro–Atlantic region. Table 1 shows the skills of the forecasts for the extreme-event index for each EOF of this region. The skill is measured in terms of correlation between predicted and analysed time series of indices of extreme events for each Euro–Atlantic PC. We can compare these values with those presented in PMB for the forecast scores for the four PCs. A substantial increase with respect to the scores for the PCs can be seen in the cases of EOF1 and EOF3, some improvement in the case of EOF2, but a large decrease in the case of EOF4 . The large decrease in the score of EOF4 suggests that, although the model was able to capture the sign of the seasonally averaged pattern, it did not capture its amplitude correctly. The large positive scores obtained for EOF1 and EOF3 indicate that the strong zonal bias prevents the model from producing the analysed blocking events, although the model reproduces, to a sufficiently good degree, the analysed interannual variability of the index.

The problems that the model has in correctly representing blocking frequency variability reflect directly on the lack of variability in the predicted frequency of storms. Figure 7 shows the composites of cyclone frequency including the data from all the ensemble members as was done for blocking composites in Fig. 5. We notice that these composites are substantially less noisy than those computed from ERA, due to the greater averaging obtained by including all ensemble members. A comparison between the observed (Fig. 4) and the modelled climatologies of large-cyclone frequency during ERA years shows that they are in good agreement. However, while in the case of the composites for the Pacific patterns it is possible to identify substantial deviations from climatological values, in the case of Euro–Atlantic patterns the model is always close to climatology.

5. Further description of results

Next we want to check how the model represents the anomalous planetary-wave generation and propagation over the Atlantic area during months characterized by high values of blocking frequency over the Atlantic. In Fig. 8, we show composites of generalized Eliassen–Palm fluxes (Plumb 1985; Karoly *et al.* 1989) together with composites of Rossby-wave sources for the patterns we are focusing on.

The importance of the Rossby-wave source in the generation of extra-tropical planetary waves was discussed by Sardeshmukh and Hoskins (1988) who defined it from a simplified form of the vorticity equation,

$$\frac{\partial \zeta}{\partial t} + \overline{v}_\psi \nabla(f+\zeta) = -(f+\zeta)D - \overline{v}_\chi \nabla(f+\zeta) \tag{1}$$

where overbars indicate time averages over one month, $\overline{v}_\psi$ and $\overline{v}_\chi$ are the rotational and divergent components of the horizontal wind, respectively, ζ is the relative vorticity, f is the Coriolis parameter, and D the horizontal wind divergence. The Rossby-wave source is defined as the right-hand side (r.h.s.) of Eq. (1). For extra-tropical, equivalent barotropic anomalies, the stretching term (first on the r.h.s.) acts as a damping term. This term can be eliminated by combining the vorticity and thermodynamic equations into a prognostic equation for quasi-geostrophic PV. The vorticity advection by the divergent

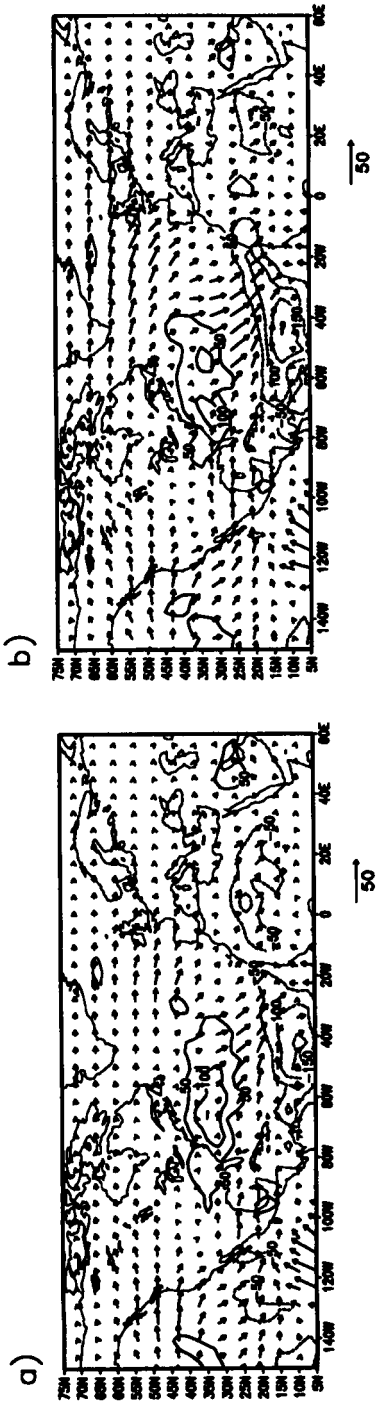

Figure 8. Composites of generalized Eliassen–Palm flux (arrows, $m^2 s^{-2}$) and of Rossby-wave source for those months in which the ATL-EOF1 ((a) and (c)) and ATL-EOF3 ((b) and (d)) are less than 0.67 for ECMWF re-analyses ((a) and (b)) and winter ensemble data ((c) and (d)). Contour interval is $50 \times 10^{-13} s^{-2}$. (See text for further explanation.)

wind, the second term on the r.h.s., represents the Rossby-wave source. This term has a substantial value close to the poleward border of the Hadley cell where the flow is still divergent and the meridional gradient of absolute vorticity is strongest. We computed its value at 200 mb and obtained composites using the same procedure used for the blocking frequencies shown in Fig. 5. The data used to compute these quantities are taken from ERA (Figs. 8(a) and (b)) and from the model (Figs. 8(c) and (d)).

For both patterns, the observed flow presents a substantial convergence of wave-action fluxes west of Mexico. Wave action is then partially propagated into the Gulf Stream region, enters a region of large positive Rossby-wave source situated at the entrance of the Atlantic storm-track, and finally dies out toward the east tropical Atlantic where a large sink of Rossby-wave activity is located, due to the relatively cooler water close to the west coast of Africa along the equator. The model largely underestimates both the wave-action convergence over the east tropical Pacific and the two Rossby-wave source extremes over the Atlantic. The final result is an underestimation of the intensity of E–P fluxes and a poor representation of their patterns. In both cases, we also notice a distinct decoupling in the wave-action propagation between mid high latitudes and the tropics over North America and the western North Atlantic, although a large region of convergence is present over Europe, possibly connected with the large Rossby-wave sink previously mentioned.

Looking in more detail, in the case of the analysed west Atlantic blocking (ATL-EOF1), very little, if any, propagation of wave action from mid-latitude Pacific to mid-latitude Atlantic can be seen, and the pattern seems to be more locally generated. In the case of the European blocking (ATL-EOF3), there is some propagation of wave action between the two sectors through high latitudes. In the latter case, the signal is locally confined under the southern tip of Greenland, where it is amplified, and reaches the region surrounding the British Isles with a substantial amplitude. The west Atlantic blocking is also associated with stronger Rossby-wave extremes: the positive source off the North American east coast is more pronounced and the sink over the tropical east Atlantic extends well into the African continent. On the other hand, the European blocking is associated with more spatially confined Rossby-wave extremes, but the sink over the east tropical Atlantic is much stronger than in the other case. This result agrees with Hoskins and Sardeshmukh (1987) who observed the presence of anomalously cold water in the equatorial east Atlantic during the strong blocking events of winter 1985/86.

The model does not reproduce most of these features (Figs. 8(c) and (d)). It represents the wave-action flux convergence over Mexico to some extent only in the European blocking case, while in the west Atlantic blocking case we can notice a signature of the extension of the Rossby-wave sink into the African continent. There is also a signature of propagation of wave action from the Pacific to the Atlantic mid-latitude sector in the case of the European blocking, but the signal is not confined south of Greenland as in the observed data it is dispersed and reaches the north-west coasts of Spain and France, suggesting a tendency to shift the centre of the anomaly to the south of its observed location.

We conclude that both the climatology of the large-scale flow and its variability are poorly represented by the model. The model data at hand do not allow the identification of the specific role of each component in the dynamics associated with the onset and mantainance of blocking, and with the generation of model errors. Therefore, we defer this task to more accurate and focused future studies.

We remember here the suggestion by Michelangeli and Vautard (1998) that an adequate representation of the nonlinear interaction between the transients and the quasi-stationary features of the large-scale flow could be essential for an appropriate

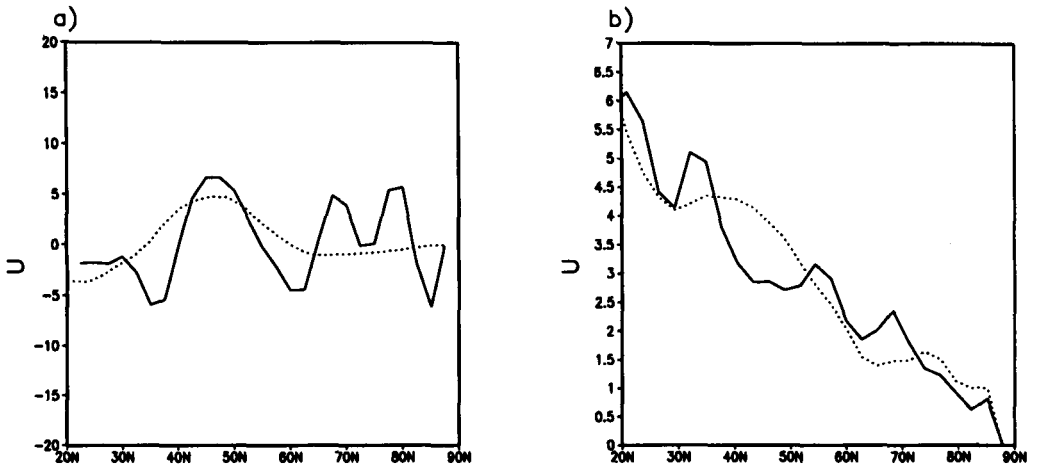

Figure 9. (a) Composites of model-error 200 mb zonal wind (dotted line) and eddy momentum flux convergence (solid line) averaged over the sector 270°E–0°E for months in which ATL-EOF1 is smaller than −0.67. (b) Composites of refraction index for ECMWF re-analyses (solid line) and winter ensemble data (dotted line) for months in which ATL-EOF3 is smaller than −0.67. (See text for further explanation.)

representation of blocking. A too strong zonal flow implies stronger eddies and, therefore, stronger eddy momentum flux convergence, which eventually will reinforce the basic zonal flow. The region in which the model error in the zonal wind is largest is located downstream of the Atlantic storm-track, and this region coincides with the region of maximum transient eddy momentum flux convergence. An excessive amplitude of the jet stream can imply erroneous values of the planetary-wave refraction index, and in turn prevent a correct propagation of the planetary waves. The relevance of this process would imply the presence of strongly nonlinear effects of the transients on the large-scale flow circulation. We show in Fig. 9 the composites of refraction index (Held 1983) for the sector from 270°W to Greenwich for both ERA and ensemble experiments (Fig. 9(b)), together with the composite of the model error in the 200 mb zonal flow and the geostrophic transient eddy momentum flux convergence, forcing the zonal wind, both averaged over the same domain (Fig. 9(a)). The only daily data available to us are the daily 500 mb geopotential height data, and that is the level at which the eddy momentum flux convergence was evaluated. We are aware that the eddy momentum flux convergence reaches its maximum value at higher levels (between 300 and 200 mb) but it is also known that the value of this quantity usually does not change sign between 500 and 200 mb, only intensifies with height.

From Fig. 9(a), we notice that the composite of the zonal-wind model error reaches a maximum at about 45°N, which coincides with the core of the mid-latitude upper-tropospheric jet. This maximum is accompanied by two relative minima on both sides of the jet. This maximum also coincides with the maximum of positive model error in the eddy momentum flux convergence, together with two regions of negative error on both sides. While the model error in the zonal wind amounts to less than 10% of actual wind intensity, the model error in the eddy momentum flux amounts to over 100% of the actual flux intensity at 45°N. The presence of a steeper jet maximum produces larger values in the refraction index about the jet maximum in the model, with respect to observations, as can be seen in Fig. 9(b). This feature prevents the model from effectively confining large-scale waves north of 50°N.

6. CONCLUSIONS

We have presented a detailed description of the regional large-scale patterns of variability over both the Euro–Atlantic and the Pacific regions, highlighting in all cases the relation between large-scale patterns and local weather regimes, namely 'blocked' and 'zonal' regimes. In both regions, we have identified the presence of blocking patterns maintained by distinct dynamical mechanisms. The European blocks are correlated with larger-than-normal transient PV transport upstream of them, while blocks associated with the NAO are not. We have found that the NAO has a distinct planetary character which agrees with the recent results by Thompson and Wallace (1998).

We have analysed the skill of blocking-frequency winter ensemble predictions for each of the Euro–Atlantic and Pacific patterns. Generally, the model has higher skill over the Pacific region, in accordance with the results obtained by other authors (e.g. Tracton *et al.* 1989). However, the model has a distinct bias towards stronger zonal mid-latitude flow with respect to verifying analyses, over both the northern Atlantic and the Pacific.

More information was obtained by defining an index of extreme events for each of the Euro–Atlantic patterns: in the case of patterns correlated with blocking, the model is able to predict the evolution of this index much better than the evolution of the principal components from which the index is derived. The improvement is particularly impressive in the case of the European blocking whose index of extreme events proved to be highly correlated with the NAO during the ERA years. A comparison between the ERA data and the model suggested that the model does not reproduce adequately the Rossby-wave extremes over the Atlantic.

ACKNOWLEDGEMENTS

The work of V. Pavan was supported by the Commission of the European Communities under project ENV4-CT95-0109 (PROVOST). The authors are grateful to Dr Molteni for many useful discussions, to Dr Anderson, and to an anonymous reviewer, whose suggestions have greatly helped to focus and improve the quality of this paper.

REFERENCES

Barnston, A. G. and Livezey, R. E. 1987 Classification, seasonality and persistence of low-frequency atmospheric circulation patterns. *Mon. Weather Rev.*, **115**, 1083–1126

Branković, Č. and Molteni, F. 1997 Sensitivity of the ECMWF model wintertime climate to model formulation. *Clim. Dyn.*, **13**, 75–101

Branković, Č. and Palmer, T. N. 2000 Seasonal skill and predictability of ECMWF PROVOST ensembles. *Q. J. R. Meteorol. Soc.*, **126**, 2035–2067

Corti, S., Giannini, A., Tibaldi, S. and Molteni, F. 1997 Patterns of low-frequency variability in a three-level quasi-geostrophic model. *Clim. Dyn.*, **13**, 883–904

D'Andrea, F., Tibaldi, S., Blackburn, M., Boer, G., Déqué, M., Dix, M. R., Dugas, B., Ferranti, L., Iwasaki, T., Kitoh, A., Pope, V., Randall, D., Roeckner, E., Straus, D., Stern, W., Van der Dool, H. and Williamson, D. 1998 Northern Hemisphere atmospheric blocking as simulated by 15 atmospheric general circulation models in the period 1979–1988. *Clim. Dyn.*, **14**, 385–407

Dole, R. M. 1983 'Persistent anomalies of the extratropical Northern Hemisphere wintertime circulation'. Pp. 95–109 in *Large-scale dynamical processes in the atmosphere*. Eds. B. J. Hoskins and R. P. Pearce, Academic Press, Inc. (London), Ltd., UK

Dole, R. M. 1986 Persistent anomalies of the extratropical Northern Hemisphere wintertime circulation: geographical distribution and regional persistent characteristics. *Mon. Weather Rev.*, **114**, 178–207

Ferranti, L., Molteni, F. and Palmer, T. N. 1994 Impact of localized and extra-tropical SST anomalies in ensembles of seasonal GCM integrations. *Q. J. R. Meteorol. Soc.*, **120**, 1613–1645

Gibson, J. K., Kallberg, P., Uppala, S., Hernandez, A., Nomura, A. and Serrano, E. 1997 'ECMWF re-analysis. Project report series.1.ERA description'. European Centre for Medium-Range Weather Forecasts, Reading, UK

Green, J. S. A. 1977 The weather during July 1976: some dynamical considerations of the drought. *Weather*, **32**, 120–128

Held, I. M. 1983 'Stationary and quasi-stationary eddies in the extratropical troposphere: theory'. Pp. 127–168 in *Large-scale dynamical processes in the atmosphere*. Eds. B. J. Hoskins and R. P. Pearce, Academic Press, Inc. (London), Ltd., UK

Hoskins, B. J. and Karoly, D. J. 1981 The steady linear response of a spherical atmosphere to thermal and orographic forcing. *J. Atmos. Sci.*, **38**, 1179–1196

Hoskins, B. J. and Sardeshmukh, P. D. 1987 A diagnostic study of the dynamics of the northern hemisphere winter of 1985–86. *Q. J. R. Meteorol. Soc.*, **113**, 759–778

Hurrell, J. W. 1996 Influence of variations in extratropical wintertime teleconnections on northern hemisphere temperatures. *Geophys. Res. Lett.*, **23**, 665–668

Hurrell, J. W. and van Loon, H. 1997 Decadal variations in climate associated with the North Atlantic oscillation. *Clim. Change*, **36**, 301–326

Karoly, D. J., Plumb, R. A. and Ting, M. 1989 Examples of the horizontal propagation of quasi-stationary waves. *J. Atmos. Sci.*, **46**, 2802–2811

Kimoto, M. and Ghill, M. 1993 Multiple flow regimes in the northern hemisphere winter. Part I: methodology and hemispheric regimes. *J. Atmos. Sci.*, **40**, 2625–2643

Legras, B. and Ghil, M. 1985 Persistent anomalies, blocking and variations in atmospheric predictability. *J. Atmos. Sci.*, **42**, 433–471

Michelangeli, P.-A. and Vautard, R. 1998 The dynamics of Euro–Atlantic blocking onsets. *Q. J. R. Meteorol. Soc.*, **124**, 1045–1070

Michelangeli, P.-A., Vautard, R. and Legras, B. 1995 Weather regimes: recurrence and quasi-stationarity. *J. Atmos. Sci.*, **52**, 1237–1256

Molteni, F. and Corti, S. 1998 Long-term fluctuations in the statistical properties of low-frequency variability: Dynamical origin and predictability. *Q. J. R. Meteorol. Soc.*, **124**, 495–526

Nakamura, H., Nakamura, M. and Anderson, J. L. 1997 The role of high- and low-frequency dynamics in blocking formation. *Mon. Weather Rev.*, **125**, 2074–2093

Palmer, T. N. and Anderson, D. L. T. 1994 The prospects for seasonal forecasting—a review paper. *Q. J. R. Meteorol. Soc.*, **120**, 755–793

Pavan, V. and Doblas-Reyes, F. 2000 Multi-model seasonal hindcasts over the Euro–Atlantic: skill scores and dynamic features. *Clim. Dyn.*, in press

Pavan, V., Molteni, F. and Branković, Č. 2000 Wintertime variability in the Euro–Atlantic region in observations and in ECMWF seasonal ensemble experiments. *Q. J. R. Meteorol. Soc.*, **126**, 2143–2173

Plaut, G. and Vautard, R. 1994 Spells of low-frequency oscillations and weather regimes in the northern hemisphere. *J. Atmos. Sci.*, **51**, 210–236

Plumb, R. A. 1985 On the three-dimensional propagation of stationary waves. *J. Atmos. Sci.*, **42**, 217–229

Rogers, J. C. 1990 Patterns of low-frequency monthly sea level pressure variability (1899–1989) and associated wave cyclone frequencies. *J. Climate*, **3**, 1364–1379

Sardeshmukh, P. D. and Hoskins, B. J. 1988 Generation of global rotational flow by steady idealized tropical divergence. *J. Atmos. Sci.*, **45**, 1128–1251

Shutts, G. J. 1986 A case study of eddy forcing during an Atlantic blocking episode. *Adv. Geophys.*, **29**, 135–161

Thompson, D. W. J. and Wallace, J. M. 1998 The arctic oscillation signature in the wintertime geopotential height and temperature fields. *Geophys. Res. Lett.*, **25**, 1297–1300

Tibaldi, S. and Molteni, F. 1990 On the operational predictability of blocking. *Tellus*, **42A**, 343–365

Tibaldi, S., Tosi, E., Navarra, A. and Pedulli, L. 1994 Northern and southern hemisphere seasonal variability of blocking frequency and predictability. *Mon. Weather Rev.*, **122**, 197–200

Tracton, M. S., Mo, K., Chen, W., Kalnay, E., Kistler, R. and White, G. 1989 Dynamical extended range forecasting (DERF) at the National Meteorological Center. *Mon. Weather Rev.*, **117**, 1604–1635

Vautard, R. 1990 Multiple weather regimes over the North Atlantic: analysis of precursors and successors. *Mon. Weather Rev.*, **118**, 2056–2081

Wallace, J. M. and Gutzler, D. S. 1981 Teleconnections in the geopotential height field during the northern hemisphere winter. *Mon. Weather Rev.*, **109**, 784–812